Modeling Subsea Pipeline Movement Subjected to Submarine Debris-Flow Impact

Xuesheng Qian, A.M.ASCE[1]; and Himangshu S. Das, M.ASCE[2]

Abstract: Deepwater pipelines are susceptible to destructive impacts from submarine debris flows. Understanding the subsea pipeline movement driven by submarine debris flow is critical to the optimization of pipeline routes and mitigation of submarine geohazards. In this paper, a coupling model of submarine debris flow with pipeline interaction is presented to investigate pipeline movement subjected to debris flow impact. The modeling domain of debris flow is represented by a structured grid system with discretized grid nodes. The dynamic properties of debris flow, such as velocities and heights, are calculated at each grid node. The pipeline is discretized into finite elements. Each element consists of two pipe nodes at the ends. The coordinates of each pipe node are determined using a particle tracking algorithm. The velocities of debris flow at the location of each pipe node are interpolated from the debris flow model and then converted to impact forces applied on each pipe node. An empirical formulation is proposed to estimate the displacements of each pipe node from a given Young's modulus of pipe material and impact force applied by debris flow. The empirical relationship is developed from a series of numerical simulations conducted with the commercial software ABAQUS. The numerical simulations are performed using a simple model configuration subjected to uniformly distributed impact forces. Later, the coupled model is applied to two schematized cases representing continental shelves with a uniform slope and a sinuous canyon. The effects of the Young's modulus of pipe material, initial failure height of debris flow, and the number of discretized pipe nodes on pipeline movement are investigated through a series of parametric studies. **DOI: 10.1061/(ASCE)PS.1949-1204.0000386.**

Author keywords: Subsea pipeline; Submarine debris flow; Pipeline movement; Strain and stress; Semiempirical method.

Introduction

Subsea pipeline systems are connected pipes that usually transport oil and gas from offshore production platforms to onshore destinations. Sometimes these pipelines must be routed up along the continental slope, often through areas where geohazards may exist. Submarine landslides and their subsequent debris flows represent one of the most significant geohazards. They pose devastating threats to offshore installations, especially pipelines due to their long span and low structural resistance. To optimize subsea pipeline routes and minimize seafloor geologic risks, it is of crucial importance to quantify pipeline movements subjected to potential submarine debris flow impacts.

Since the failure of three platforms in the Gulf of Mexico during Hurricane Camille in 1969, many techniques have been developed to assess impact forces arising from the interaction between mass gravity flows and seafloor infrastructures such as pipelines (Audibert and Nyman 1979; Bea and Aurora 1982). In general, this problem has primarily been investigated from three perspectives: the soil mechanics approach, fluid mechanics approach, and a unified approach of soil and fluid mechanics. The soil mechanics approach was mainly developed between the mid-1970s and the late 1980s (Zakeri 2009). In this approach, drag forces are assumed to be proportional to undrained shear strength of sliding mass, and an empirical parameter is also introduced. This parameter was initially set as a constant for simplicity (e.g., Wieghardt 1975; Towhata and Al-Hussaini 1988). However, it provides a wide range of estimations of drag forces. To reduce the uncertainty when assessing drag forces, it was later determined using power-law relations (e.g., Shcapery and Dunlap 1978; Zakeri et al. 2012). In the fluid mechanics approach, sliding soil is treated as a fully fluidized non-Newtonian fluid. In this method, it is vital to determine the drag coefficient, and only a few studies have contributed to it. Pazwash and Robertson (1975) first investigated drag forces exerted by a non-Newtonian fluid flowing around objects. Zakeri et al. (2008) set up a series of laboratory experiments to investigate debris flow impact on pipelines and developed relations between drag coefficient and non-Newtonian Reynolds number. Their experiments were complemented by extensive computational fluid dynamics (CFD) analyses (Zakeri et al. 2009). The two foregoing approaches are limited by their applicable conditions. The soil mechanics approach is more suitable to the early stage of submarine landslides, when soil strength is close to intact conditions, and the velocities of moving soil are relatively low. On the other hand, the fluid mechanics approach is most applicable to fully fluidized debris flows and turbidity currents. However, during a submarine landslide, pipelines may experience impact loadings initially from intact soil at the very early stage of the incident and subsequently from fully fluidized conditions. To capture such effects arising from the solid-to-fluid transition, Randolph and White (2012) first proposed the hybrid approach, which is a superposition of the soil and fluid mechanics approaches. This approach was validated by laboratory experiments (Sahdi et al. 2014) and the interpretation of data from CFD analyses (Liu et al. 2015). However, evaluation of

[1]Postdoctoral Researcher, Dept. of Ocean Science and Engineering, Southern Univ. of Science and Technology, Shenzhen, Guangdong 518055, China; formerly, Ph.D. Student, Dept. of Civil and Environmental Engineering, Jackson State Univ., Jackson, MS 39217. ORCID: https://orcid.org/0000-0003-2159-9430. Email: xsq621@gmail.com

[2]Subject Matter Expert, Engineering and Construction Division, USACE, Galveston, TX 77550 (corresponding author). Email: h_shekhar@hotmail.com

Note. This manuscript was submitted on November 7, 2017; approved on December 7, 2018; published online on April 12, 2019. Discussion period open until September 12, 2019; separate discussions must be submitted for individual papers. This paper is part of the ***Journal of Pipeline Systems Engineering and Practice***, © ASCE, ISSN 1949-1190.

submarine debris flow impact on pipelines is only one of the most critical steps, and responses of pipelines subjected to debris flow impact should be further analyzed.

Many researchers have also examined the responses of buried onshore short pipes subjected to terrestrial landslides and ground subsidence (e.g., Kinash and Najafi 2012; Kouretzis et al. 2015). However, deepwater pipelines are usually laid on the seafloor and may undergo direct thrust from fast-moving mass gravity flows. In addition, the representation of structural responses in short pipes widely varies from the responses of long-span pipelines. As such, it is important to evaluate the overall responses of long-span pipelines subjected to debris flow impacts. Bruschi et al. (2006) first discussed submarine debris flow impact on the entire pipeline. Later, several researchers developed analytical solutions to analyze the integrity of whole pipelines (Parker et al. 2008; Randolph et al. 2010; Yuan et al. 2012a, b, 2015). However, the analytical model was developed based on a series of assumptions, which limit its application merely to oversimplified scenarios. To investigate the coupled interactions between debris flow and pipeline, Abeele et al. (2013) introduced a coupled Eulerian and Lagrangian method in the commercial software ABAQUS. It integrates in one framework the fluid dynamics of debris flows, interactions between debris flow and pipeline, and the structural responses of the pipeline. However, owing to its extremely high computational cost, the approach is limited to simulations of debris flow impact on the local joints of pipelines. Spinewine et al. (2013) and Ingarfield et al. (2016) suggested the coupling of a density flow model and finite-element software such as SAGE Profile (Abeele and Denis 2012) and ABAQUS. The coupled model allows dynamic loadings from density flow model to be fed into the finite-element solver. However, no efforts have been reportedly undertaken to achieve this purpose.

With increased activities in offshore drilling and mining pushing toward deeper water, the assessment of submarine debris flow impact on the integrity of pipelines is becoming increasingly important. Quantification of deepwater pipeline movement driven by debris flows provides critical information for the optimization of pipeline routes and the mitigation of submarine geohazards. As such, it is pressing to develop a new methodology to efficiently simulate the overall responses of long-span pipelines under various configurations of submarine debris flow impact. In this work, a coupling model of debris flows with pipeline interaction was developed to investigate pipeline movement due to transient impacts arising from submarine debris flows. Two schematized cases representing continental shelves with a uniform slope and a sinuous canyon are used to demonstrate the present model.

Model Descriptions

Submarine Debris Flow Model

A two-dimensional numerical model is presented to simulate debris flow. The nonlinear Herschel–Bulkley model (Herschel and Bulkley 1926) is used to describe the rheology of a debris flow:

$$\tau = \tau_Y + K\left|\frac{\partial u}{\partial z}\right|^n \quad \left|\frac{\partial u}{\partial z}\right| > 0$$
$$\tau \le \tau_Y \quad \left|\frac{\partial u}{\partial z}\right| = 0 \tag{1}$$

where τ = internal shear stress (Pa); τ_Y = yield stress (Pa); u = velocity parallel to bed (m/s); z = coordinate normal to bed; K = consistency related to dynamic viscosity μ (Pa · s); and n = model factor for shear thinning fluid. When $n = 1.0$, the nonlinear Herschel–Bulkley model is simplified to the linear Bingham model.

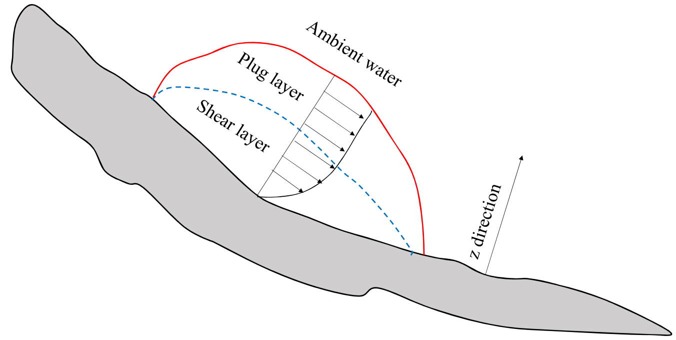

Fig. 1. Schematic view of layer definition and vertical velocity profile of submarine debris flow.

Several assumptions are made to describe the physical behavior of the problem in terms of model equations. A thin layer approximation is applied, which represents a runout distance of debris flow that is much greater than the depth. The buoyancy effect of ambient fluid on debris flow is considered. However, no mass fluxes or frictional interaction at the interface of debris flow and ambient fluid is assumed. In addition, submarine debris flow is simplified as a single-phase flow. Then the conservation equation of mass is

$$\frac{\partial H}{\partial t} + \frac{\partial UH}{\partial x} + \frac{\partial VH}{\partial y} = M \tag{2}$$

and the conservation equations of momentum along the x- and y-directions are

$$\frac{\partial UH}{\partial t} + \frac{\partial UUH}{\partial x} + \frac{\partial UVH}{\partial y} + \frac{1}{2}\frac{\rho_d - \rho_w}{\rho_d} g \frac{\partial H^2}{\partial x} + \frac{\rho_d - \rho_w}{\rho_d} gH \frac{\partial \eta}{\partial x} + \frac{\tau_{bx}}{\rho_d} = \frac{\mu}{\rho_d}\left(\frac{\partial^2 UH}{\partial x^2} + \frac{\partial^2 UH}{\partial y^2}\right) \tag{3a}$$

$$\frac{\partial VH}{\partial t} + \frac{\partial VUH}{\partial x} + \frac{\partial VVH}{\partial y} + \frac{1}{2}\frac{\rho_d - \rho_w}{\rho_d} g \frac{\partial H^2}{\partial y} + \frac{\rho_d - \rho_w}{\rho_d} gH \frac{\partial \eta}{\partial y} + \frac{\tau_{by}}{\rho_d} = \frac{\mu}{\rho_d}\left(\frac{\partial^2 VH}{\partial x^2} + \frac{\partial^2 VH}{\partial y^2}\right) \tag{3b}$$

where t = time (s); x and y = coordinates parallel to bed; U and V = depth-averaged velocities in x- and y-directions (m/s); H = height of debris flow (m); ρ_d = density of debris flow (kg/m^3); ρ_w = density of ambient fluid (kg/m^3); η = bed elevation (m); τ_{bx} and τ_{by} = bottom shear stresses in x- and y-directions (Pa); and M = rate of flow per unit area (m/s).

The debris flow is assumed to be divided into two distinct parts, the shear and plug layers (Fig. 1). In the shear layer, the shear stress exceeds the yield stress, and a parabolic velocity profile is shown. However, the plug layer presents a uniform velocity distribution. In addition, the shear stress distribution within the debris flow is assumed linear. As such, the bottom shear stress is represented as

$$\tau_b = \frac{\tau_y}{\xi} \tag{4}$$

and the nondimensional parameter $\xi \in (0, 1)$ is determined by

J. Pipeline Syst. Eng. Pract., 2019, 10(3): 04019016

$$\left(\xi+\frac{1}{n}+1\right)(1-\xi)^{\frac{1}{n}+1}-\frac{(\frac{1}{n}+1)(\frac{1}{n}+2)|U|K^{\frac{1}{n}}}{H\tau_Y^{\frac{1}{n}}}\xi^{\frac{1}{n}}=0, \xi\in(0,1) \tag{5}$$

This equation leads to a unique solution ξ with respect to the specific range of $\xi \in (0,1)$. The Newton–Raphson iteration method is used to solve the preceding equation. Finally, the explicit finite difference method is used to solve Eqs. (2) and (3). More details on the mathematical derivation of Eq. (5) and numerical schemes used to solve Eqs. (2) and (3) are found in Qian and Das (2019).

Pipeline Movement Model

The pipeline is discretized into finite elements (Fig. 2). Each element is composed of two pipe nodes at the ends. A spring is used to connect these two nodes. However, the effect of this spring is neglected, and thus these pipe nodes do not interact with each other. The coordinates of each pipe node at each time step are determined using a particle tracking algorithm (PTA), which is introduced in the next subsection. The modeling domain is represented by a structured grid system with discretized grid nodes. The real-time velocities and heights of debris flow at each grid node are calculated from the debris flow model. The debris flow velocities at the location of each pipe node are interpolated from those at the neighboring grid nodes. Herein, the inverse distance weighting method is used for the interpolation

$$\underline{U}=\frac{\sum_{i=1}^{n}\frac{U_i}{r_i}}{\sum_{i=1}^{n}\frac{1}{r_i}} \tag{6}$$

where $\underline{U}$ = interpolated velocity of debris flow at location of each pipe node (m/s); U_i = velocity of debris flow at neighboring grid node (m/s); r_i = distance between pipe node and grid node; and n = number of neighboring grid node. If $n=1$, the pipe node is located at the grid node; if $n=2$, it is at the grid edge; and if $n=4$, it is at the grid face.

In the pipeline movement model, the reaction forces on debris flow due to pipeline movement is ignored. As a result, this model is a one-way coupled interaction model, which means that debris flow causes the pipe to move. However, pipeline movement has no effects on debris flow, which is an assumption in the current model subject to improvement in the future. The velocities of debris flows are converted to impact forces applied on each pipe node. The conversion procedures are illustrated as follows. With interpolated velocities of debris flows at the exact locations of each pipe node, one can obtain the shear strain rate as

$$\gamma=\frac{U}{D} \tag{7}$$

where γ = shear strain rate (s^{-1}); and D = diameter of pipe node (m). Based on the Herschel–Bulkley rheological model, the shear stress is readily calculated as

$$\tau=\tau_Y+K\gamma^n \tag{8}$$

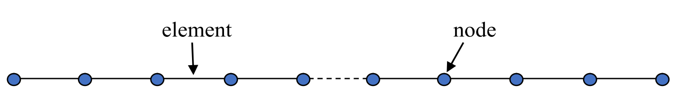

Fig. 2. Discretization of pipeline.

where τ = shear stress (Pa). The non-Newtonian Reynolds number is then obtained from

$$\mathsf{R}=\frac{\rho_d \underline{U}^2}{\tau} \tag{9}$$

where R is the non-Newtonian Reynolds number. The drag coefficient is obtained using the following relationship established from laboratory experiments (Zakeri et al. 2008) and later validated using numerical simulations (Zakeri et al. 2009):

$$C_D=a+\frac{b}{\mathrm{Re}^c} \tag{10}$$

where C_D = drag coefficient; and a, b, and c = empirical coefficients obtained from laboratory experiments (Zakeri et al. 2008). The debris flow impact forces acting on the pipe nodes are estimated using

$$F_D=\frac{1}{2}\rho_d\cdot C_D\cdot \underline{U}^2\cdot A \tag{11}$$

where F_D = debris flow impact force (N); and A = projected area of pipe node (m^2). With estimated impact forces applied on the pipe nodes, one can readily predict their displacements within a single time step. Then the new coordinates for each pipe node are updated. After that, their locations are redetermined using the PTA, and similar procedures are repeated during the next time step.

Particle Tracking Algorithm

As previously stated, the modeling domain of debris flow is discretized with a structured grid system. The pipeline is discretized into many pipe nodes. The locations of each pipe node overlying the grid system have four scenarios, i.e., grid nodes, grid edges in the I-direction, grid edges in the J-direction, and grid faces. An algorithm is devised to locate the positions of pipe nodes in the grid system. Herein, the procedures are briefly illustrated. First, calculate the distances $dist1$, $dist2$, $dist3$, and $dist4$ between pipe node (m) and grid nodes (i,j), $(i+1,j)$, $(i,j+1)$, and $(i+1,j+1)$, respectively. Second, calculate the distances between grid nodes (i,j), $(i+1,j)$, $(i,j+1)$, and $(i+1,j+1)$. Herein, $dist5$ is the distance between (i,j) and $(i+1,j)$, $dist6$ is between (i,j) and $(i,j+1)$, $dist7$ is between $(i+1,j)$ and $(i+1,j+1)$, and $dist8$ is between $(i,j+1)$ and $(i+1,j+1)$. Finally, determine the positions of each pipe node using the following criteria. If $dist1=0$, the pipe node is located at the grid node. If $dist1+dist2-dist5=0$, it is at the grid edge in the I-direction. If $dist1+dist3-dist6=0$, it is at the grid edge in the J-direction. Otherwise, it is at the grid face.

At the initial time step, an intensive search is performed throughout the entire grid system to identify the initial positions of each pipe node. After completion, the search is confined to the neighboring 16 grid nodes for the remaining time steps. The explanation for this is given as follows. In the submarine debris flow model, the Courant–Friedrichs–Lewy condition requires that time steps be less than a certain value in the explicit time-marching problem. If this condition is satisfied, the running distances of the debris flow should not exceed the size of a single grid. Since the velocities of each pipe node cannot be greater than those of the debris flow, pipe nodes under any circumstances cannot be displaced outside the neighboring grids. Therefore, after the first time step, the search is confined to the neighboring 16 grid nodes, i.e., $(i-1,j-1)$,

J. Pipeline Syst. Eng. Pract., 2019, 10(3): 04019016

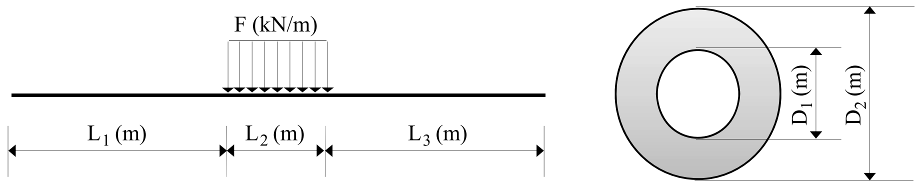

Fig. 3. Schematic of pipeline subjected to submarine debris flow impact. $L_1 = 695$ m, $L_2 = 10$ m, $L_3 = 695$ m, $D_1 = 0.4$ m, and $D_2 = 0.5$ m.

$(i, j-1)$, $(i+1, j-1)$, $(i+2, j-1)$, $(i-1, j)$, (i, j), $(i+1, j)$, $(i+2, j)$, $(i-1, j+1)$, $(i, j+1)$, $(i+1, j+1)$, $(i+2, j+1)$, $(i-1, j+2)$, $(i, j+2)$, $(i+1, j+2)$, and $(i+2, j+2)$.

Empirical Formulation

Prediction of pipe node displacement within a single time step is performed using an empirical relation. Herein, the derivation of this empirical relation is elaborated as follows. A simple modeling configuration is developed to conduct a series of numerical simulations in the commercial software ABAQUS (Fig. 3). The pipeline is laid on the seafloor with fixed ends. It has a length of 1,400 m and a circular cross section with a 0.5 m outside diameter and 0.4 m inside diameter. The uniformly distributed impact force arising from the submarine debris flow is applied to the pipeline. The impact section is located at the center of the pipeline and has a length of 10 m. The magnitudes of impact force vary from 0.1 to 10.0 kN/m. The justification for this setting is given as follows. Assuming the debris flow behaves as a Bingham fluid with a yield strength of 200 Pa, dynamic viscosity of 58 Pa · s, bulk density of 1,450 $\mathrm{kg/m^3}$, and velocity varying from 0.3 to 5 m/s (Das 2012), one finds that the non-Newtonian Reynolds number will be in a range of 0.5 and 46 and the corresponding impact force will be between 0.7 and 12.5 kN/m. As such, it is reasonable to set the magnitudes of impact force in a range of 0.1–10.0 kN/m. The impact force is continuously applied on the pipe section during a simulation period of 9 s. In ABAQUS, the pipeline is set as a two-dimensional deformable beam with a circular cross section. It is assumed to be elastic material with a Young's modulus varying from 0.7×10^6 to 0.7×10^9 Pa. The Poisson's ratio is set at 0.34, and the density is 970 $\mathrm{kg/m^3}$. The pipeline is discretized into a total of 999 elements.

Based on the numerical simulations, an empirical relation is established to estimate the displacements of each pipe node from a given Young's modulus of pipeline material and impact force. The detailed procedures are elaborated as follows. First, the relation is proposed to estimate the average strain based on a given Young's modulus and impact force:

$$\underline{S} = f(\underline{E}, \underline{F}) \tag{12}$$

$$\underline{E} = \frac{ED^2}{mg} \tag{13}$$

$$\underline{F} = \frac{F}{mg} \tag{14}$$

where $\underline{S}$ = averaged strain; E = Young's modulus of pipe material (Pa); $\underline{E}$ = normalized Young's modulus; F = impact force imposed by debris flow (N); $\underline{F}$ = normalized impact force; D = outside diameter of pipe (m); m = mass of pipe per unit length (kg); and g = gravitational acceleration ($\mathrm{m/s^2}$). The relationship between average strain and normalized impact force is shown in Fig. 4. It is found

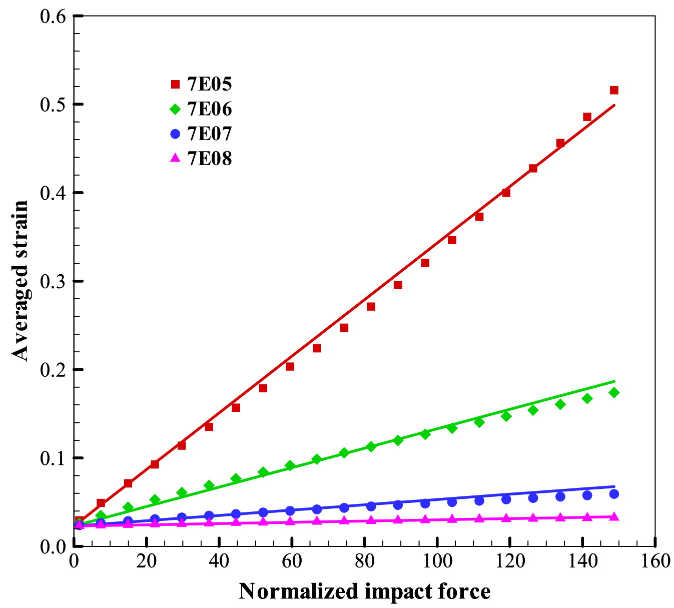

Fig. 4. Relation between normalized impact force and average strain.

that, for a given Young's modulus, the average strain is linearly proportional to the normalized impact force:

$$\underline{S} = K_1 \cdot \underline{F} + \underline{S_0} \tag{15}$$

where $\underline{S_0}$ = constant intercept of average strain; and K_1 = slope of linearized Eq. (15), which presents a power-law relation with the normalized Young's modulus (Fig. 5):

$$K_1 = C_1 \cdot \underline{E}^{C_2} \tag{16}$$

where C_1 and C_2 = empirical parameters determined from numerical simulations.

Second, an empirical relation is proposed to estimate the average strain based on a given Young's modulus and the known maximum displacement:

$$\underline{S} = f(\underline{E}, \underline{D}) \tag{17}$$

$$\underline{E} = \frac{ED^2}{mg} \tag{18}$$

$$\underline{D} = \frac{D_{\max}}{D} \tag{19}$$

where $D_{\max}$ = maximum displacement (m); and $\underline{D}$ = normalized maximum displacement. The relationship between the average strain and the normalized maximum displacement is shown in Fig. 6. For a given Young's modulus, the average strain is

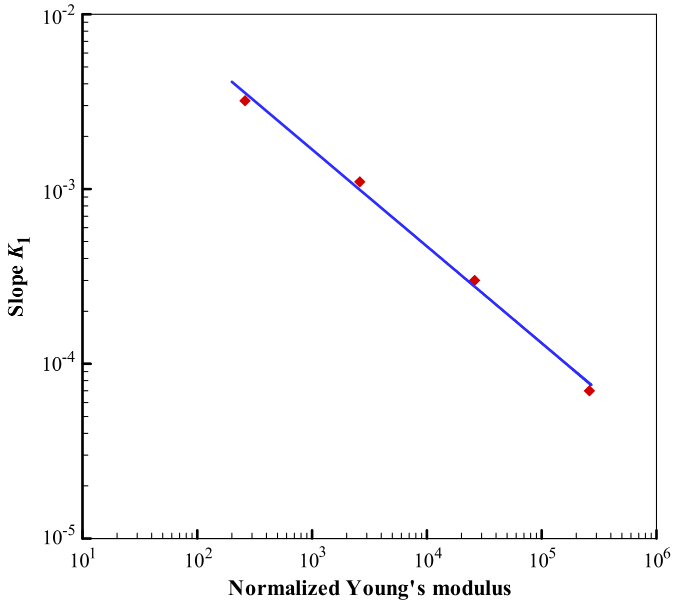

Fig. 5. Relation between normalized Young's modulus and slope K_1.

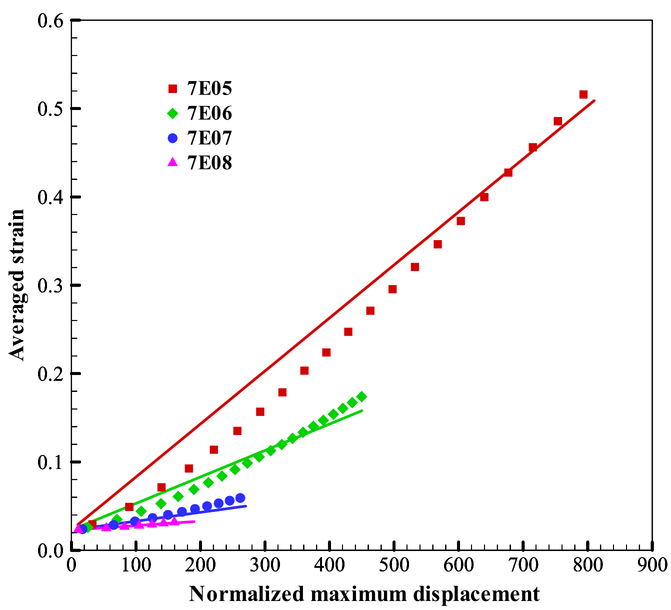

Fig. 6. Relation between normalized maximum displacement and average strain.

assumed to be linearly proportional to the normalized maximum displacement

$$\underline{S} = K_2 \cdot \underline{D} + \underline{S}_0 \tag{20}$$

where K_2 = slope of Eq. (20), which presents a power-law relation with the normalized Young's modulus (Fig. 7)

$$K_2 = C_3 \cdot \underline{E}^{C_4} \tag{21}$$

where C_3 and C_4 = empirical parameters determined from numerical simulations.

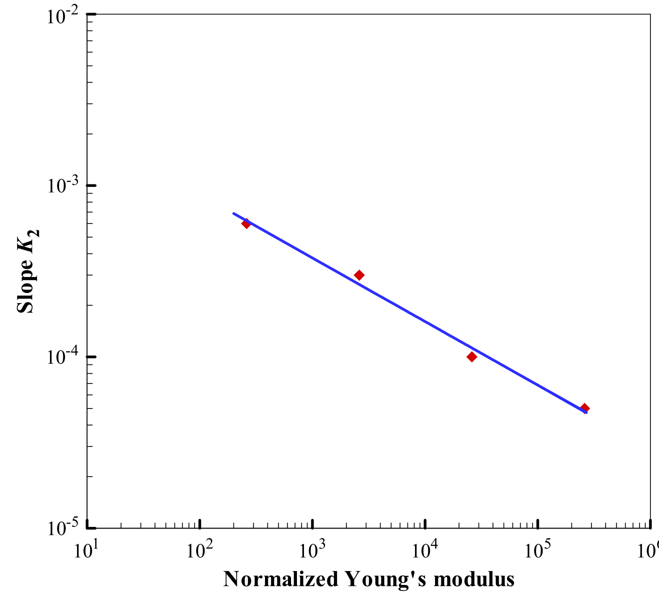

Fig. 7. Relation between normalized Young's modulus and slope K_2.

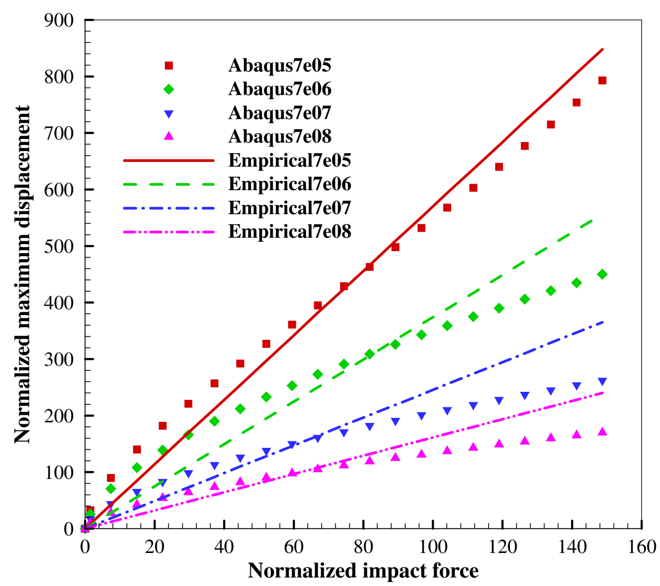

Fig. 8. Comparison of normalized maximum displacements between empirical prediction and ABAQUS model.

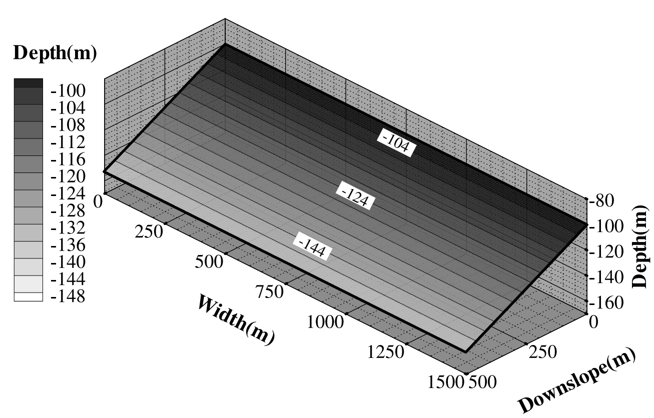

Fig. 9. Schematized continental shelf with uniform slope.

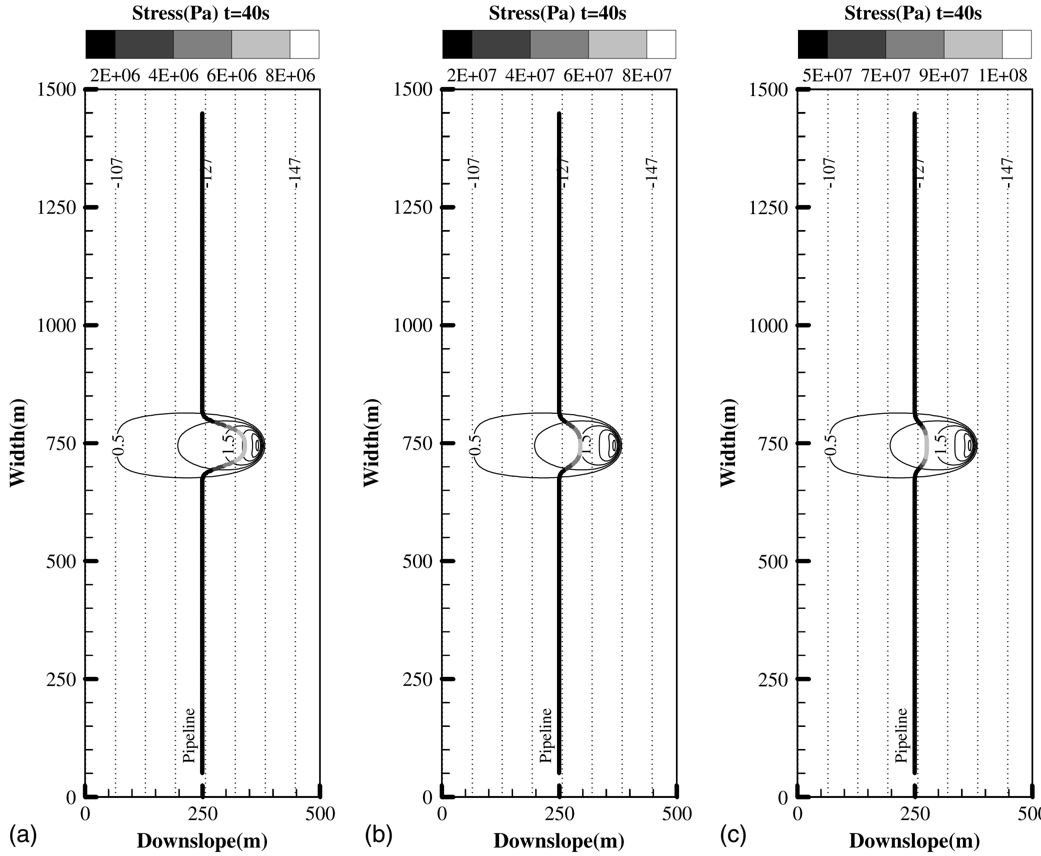

Fig. 10. Deposition patterns along with pipeline displacements over uniform slope at 40 s with initial debris height of 4 m: (a) FPVC; (b) HDPE; and (c) RPVC.

Finally, an empirical relation is obtained to estimate the displacement of a pipe node for a given Young's modulus and impact force by equating Eqs. (12) and (17), which yields

$$\underline{D} = f(\underline{E}, \underline{F}) = \frac{C_1}{C_3} \cdot \underline{E}^{C_2 - C_4} \cdot \underline{F} \tag{22}$$

where C_1, C_2, C_3, and C_4 = empirical parameters determined from numerical simulations; $\underline{E}$ = normalized Young's modulus; $\underline{D}$ = normalized maximum displacement; and $\underline{F}$ = normalized impact force. A comparison of normalized maximum displacements between the empirical prediction and ABAQUS model is shown in Fig. 8.

Model Applications

Application I: Continental Shelf with Uniform Slope

The coupled numerical model is applied to the schematized continental shelf with a uniform slope (Fig. 9). The length of the schematized domain is 1,500 m, and the width is 500 m. The slope is set at 6°. The initial deposit block is a cuboid with its centroid located at (125 m, 750 m). The width and length of the cuboid are the same and set at 100 m, and its thickness varies from 1 to 8 m. The debris flow is characterized as a Bingham fluid with a yield strength of 200 Pa and dynamic viscosity of 58 Pa · s (Das 2012). The bulk density of debris flow is 1,450 $\mathrm{kg/m^3}$. The model domain is represented by a rectangular grid system. The structured mesh size is 5×5 m. With a horizontal distance of 250 m from the shoreline, the pipeline is freely laid on the seabed and parallel to the seafloor bathymetry. The pipeline is 1,400 m in length and has a circular cross section with outside diameter of 0.5 m and inside diameter of 0.4 m. The pipeline is discretized into a total of 1,401 pipe nodes. Three different values of Young's modulus are used to represent three types of pipe material, flexible polyvinyl chloride (FPVC),

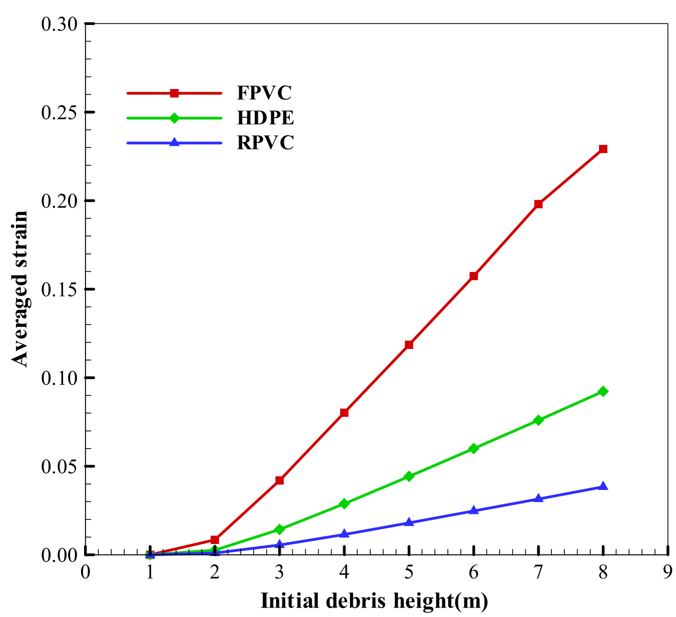

Fig. 11. Relationships between initial debris height, pipeline material, and average strain over uniform slope.

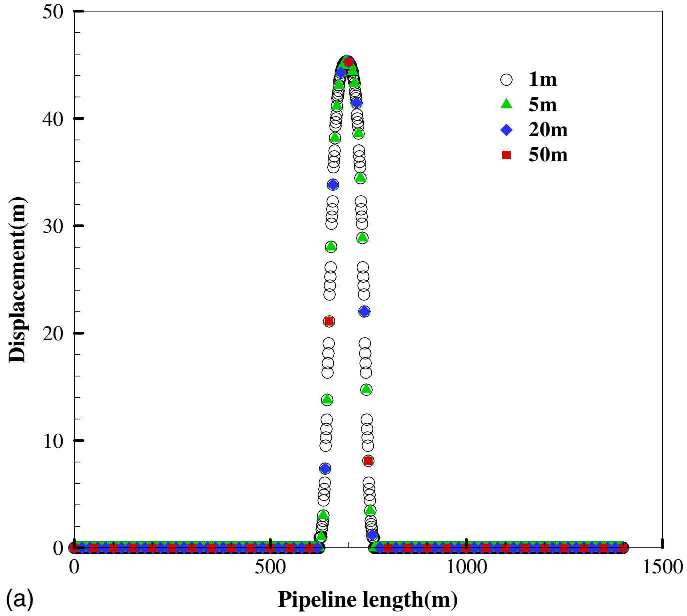

Fig. 12. Sensitivity analysis of HDPE pipeline discretization for Application I: (a) pipeline displacement; and (b) strain distribution along pipeline.

high-density polyethylene (HDPE), and rigid polyvinyl chloride (RPVC). The Young's moduli of FPVC, HDPE, and RPVC pipelines are set at 0.7×10^7, 0.7×10^9, and 0.3×10^{10} Pa, respectively. Their material densities are set at 1300.0, 970.0, and 1300.0 kg/m^3, respectively. The time step is set at 0.001 s. Each case is run for a total time of 40 s.

The debris flow deposition patterns along with the FPVC, HDPE, and RPVC pipeline displacements at 40 s are shown in Fig. 10. The distributions of stresses along the pipeline at 40 s are also displayed in the same figures. As shown in Fig. 10, the maximum stress along the pipeline arises at the same location where maximum displacement occurs. The relations between initial debris height, pipeline material, and averaged strain are shown in Fig. 11. Herein, the average strain is defined as the ratio of deformed length to initial length of pipeline. It is shown that, for a given initial failure height of debris flow, the FPVC pipeline experiences the largest average strain, whereas the RPVC pipeline represents the smallest average strain. This is due to different Young's moduli for different pipe materials. The larger the Young's modulus of the pipeline material, the smaller the average strain. In addition, it is also shown in Fig. 11 that, for a given pipeline material, the average strain of pipeline rises with the increase in initial failure height of debris

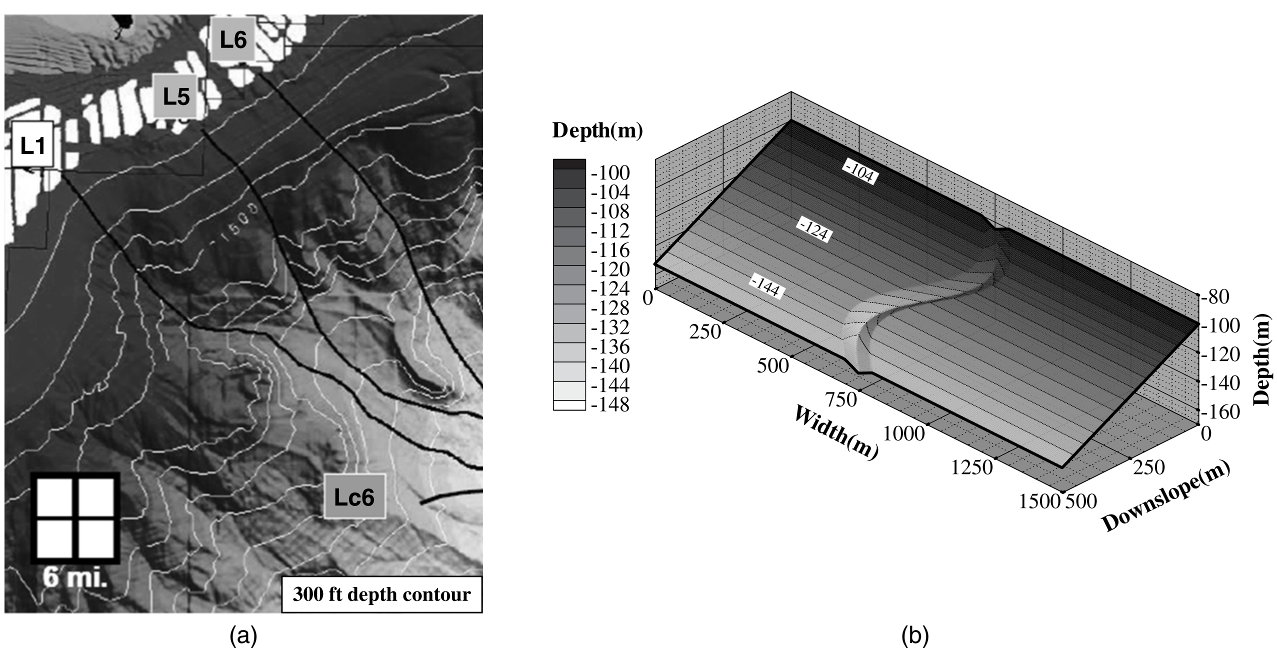

Fig. 13. (a) Canyon system in Na Kika Basin, Gulf of Mexico, where sinuosity of canyons (black lines) is obvious; and (b) schematized continental shelf with sinuous canyon.

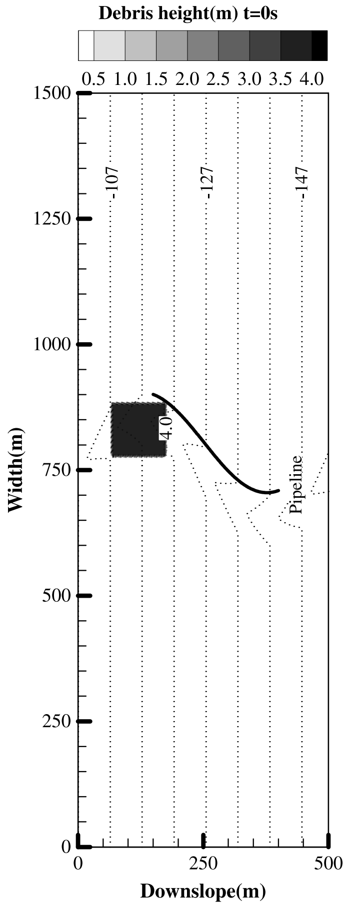

Fig. 14. Initial route of subsea pipeline along edge of sinuous canyon.

flow. Furthermore, sensitivity analysis of pipeline discretization is performed. Herein, four different distances (i.e., 1, 5, 20, and 50 m) between neighboring pipe nodes are selected to divide the HDPE pipeline. The modeling results of pipeline displacement and strain distribution along the pipeline are shown in Fig. 12. It is shown that increased displacement of pipeline will generate larger strain. It is also readily found that the modeling results are insensitive to pipeline discretization.

Application II: Continental Shelf with Sinuous Canyon

To apply the model to a real-world system, the Na Kika Basin, Gulf of Mexico, was considered (Pirmez et al. 2004) [Fig. 13(a)]. Here, the black lines labeled L1, L4, L5, and Lc6 represent the paths of steepest descent downslope along the canyons. Among them, the canyon labeled L1 presents a sinuous landform, from which the continental shelf with a sinuous canyon is schematized [Fig. 13(b)]. The geometry of the idealized domain is consistent with that described in Fig. 9. The parameter settings of debris flow and discretization of model domain are the same as described in Application I. Herein, only the geometry of a sinuous canyon is added. The midpoints at the uppermost and lowermost boundaries are selected as the starting and ending points of the thalweg of the sinuous canyon. The thalweg of the sinuous canyon is represented by a sine function of one period. The wavelength of the canyon is 500 m, and the wave amplitude is 100 m. The canyon has a V-shaped cross section with a constant side slope. The side slope is determined by the ratio of depth to width. The depth is measured at the thalweg, and the width is a horizontal deviation from the thalweg to the bank. For this canyon, the depth is 5 m, and the width is 50 m. The pipeline is initially routed along the edge of the sinuous canyon (Fig. 14). All other parameter settings of pipeline are

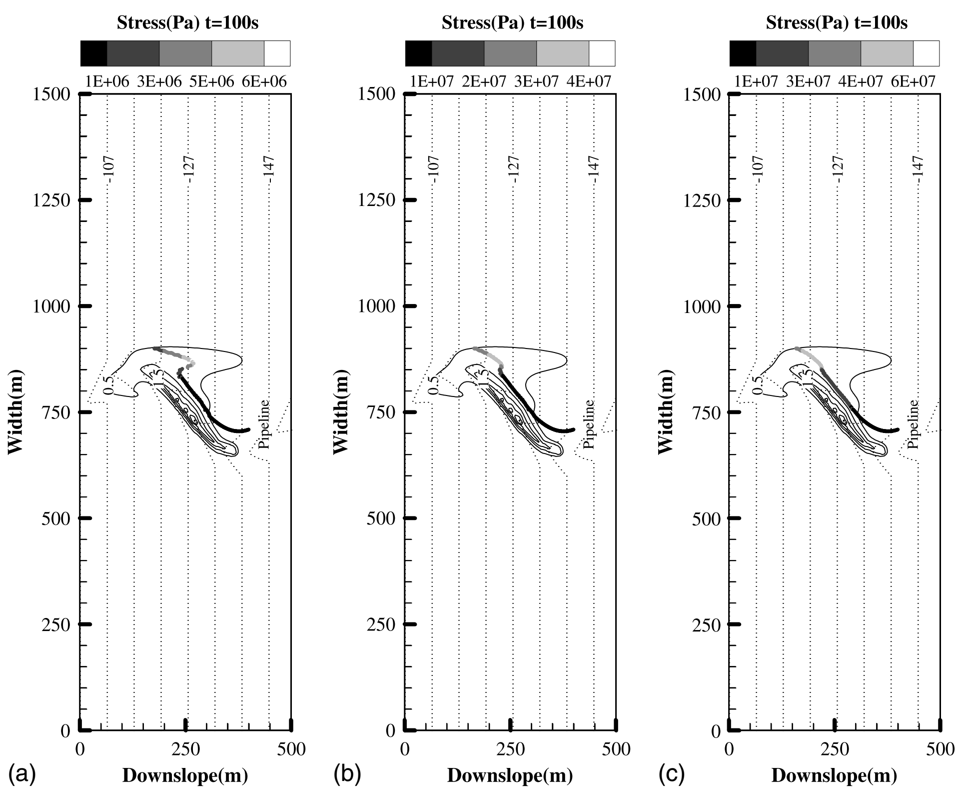

Fig. 15. Deposition patterns along with pipeline displacements over sinuous canyon at 100 s with initial debris height of 4 m: (a) FPVC; (b) HDPE; and (c) RPVC.

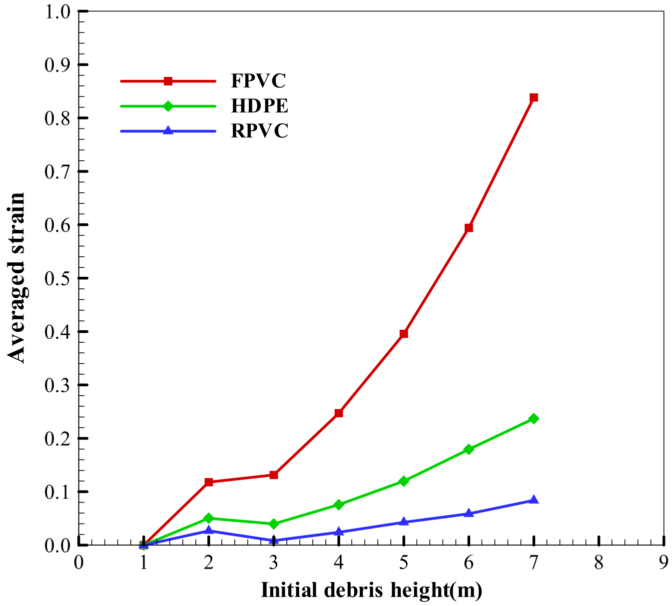

Fig. 16. Relationships between initial debris height, pipeline material, and average strain over sinuous canyon.

the same as those provided in Application I. The time step is set at 0.001 s. The coupled model is run for a total time of 100 s.

The debris flow deposition patterns along with the FPVC, HDPE, and RPVC pipeline displacements at 100 s are shown in Fig. 15. It is shown that overspills of debris flow take place. The section of pipeline located outside the canyon is significantly affected by debris overflows. The distributions of stresses along the pipeline at 100 s are also displayed in the same figures. As shown in Fig. 15, the maximum stress along the pipeline arises at the same location where maximum displacement occurs. The relationships between initial debris height, pipe material, and average strain are shown in Fig. 16. Herein, the averaged strain is defined as the ratio of the deformed length to the initial length of pipeline. Again, it is found that, for a given initial debris height, the FPVC pipeline experiences the largest average strain, and the RPVC pipeline represents the smallest average strain. This is due to the different Young's moduli of the pipeline materials. The larger the Young's modulus of the pipeline material, the smaller the average strain. In addition, it is also shown in Fig. 16 that, for a given pipeline material, the average strain of pipeline rises with the increase in initial failure height of debris flow. Sensitivity analysis of pipeline discretization is also performed in this application. Herein, the HDPE pipeline is discretized into a series of pipe nodes with four different neighboring distances (i.e., 1, 5, 20, and 50 m). Fig. 17 presents the modeling results of pipeline displacement and strain distribution along the pipeline. It is shown that a larger displacement will produce more strain in the pipeline. It is also shown that pipeline discretization has no influence on modeling results.

Concluding Remarks

A coupled model of submarine debris flow with pipeline interaction was developed to investigate pipeline movement driven by debris flow. The model was applied to two schematized cases of continental shelves with a uniform slope and a sinuous canyon. The influence of the Young's modulus of the pipe material, initial failure height of debris flow, and pipeline discretization on pipeline movement are investigated through a series of parametric studies. Modeling results showed that maximum stress along the pipeline arises at the same location where maximum displacement occurs. It is also shown that an increased Young's modulus of pipe material contributes to a reduced average strain and enhanced initial failure height of debris flow leads to increased average strain. It was further shown that modeling results were insensitive to pipeline discretization. A few limitations of the present model were identified that need to be investigated in future. For example, the pipeline is assumed to be laid on the seafloor. However, suspensions and burials of pipelines due to complex seafloor morphology and hydrodynamic conditions are very common in offshore industries. As such, the effects of pipeline suspension height should be considered. In addition, interactions between connecting pipe sections

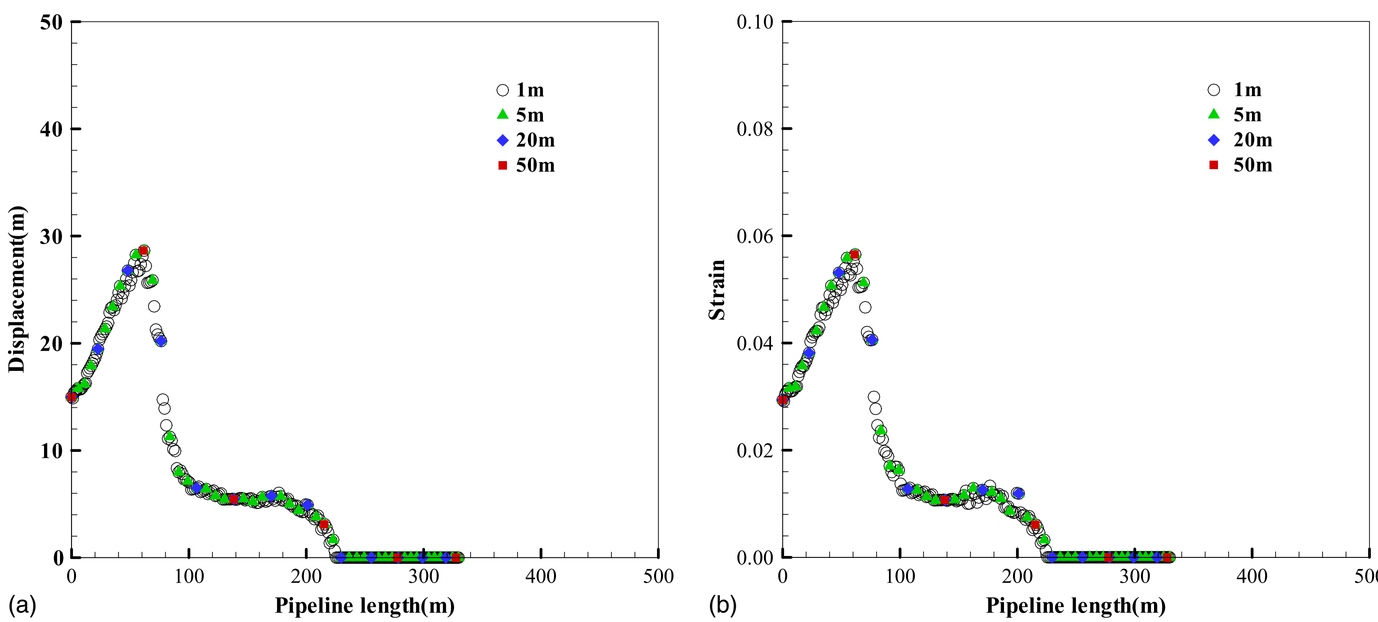

Fig. 17. Sensitivity analysis of HDPE pipeline discretization for Application II: (a) pipeline displacement; and (b) strain distribution along pipeline.

have not yet been investigated. Also, reaction forces on debris flow due to pipeline movement are neglected. Despite these limitations, the present numerical model can still serve as an efficient and practical tool to optimize pipeline routes and, thus, reduce costs and risks during pipeline construction, operation, and maintenance.

Acknowledgments

This research was supported primarily by the US Army Research Office (Grant No. W911NF1310128) and Fugro Corporation (Grant No. 636567). Partial support was also provided by the Coastal Hazards Center of Excellence and the Institute for Multimodal Transportation at Jackson State University and is greatly appreciated.

References

Abeele, F. V., and R. Denis. 2012. "Numerical modelling and analysis for offshore pipeline design, installation, and operation." *J. Pipeline Eng.* 11 (4): 273–286.

Abeele, F. V., B. Spinewine, J. C. Ballard, R. Denis, and M. Knight. 2013. "Advanced finite element analysis to tackle challenging problems in pipeline geotechnics." In *Proc., Simulia Community Conf.* Velizy-Villacoublay, France: Dassault Systemes.

Audibert, J. M. E., and K. J. Nyman. 1979. "Soil restraint against horizontal motion of pipes." *J. Geotech. Geoenviron. Eng.* 105 (12): 1555–1558.

Bea, R. G., and R. P. Aurora. 1982. "Design of pipelines in mudslide areas." In *Proc., Offshore Technology Conf.* Houston: Offshore Technology Conference.

Bruschi, R., S. Bughi, M. Spinazzè, E. Torselletti, and L. Vitali. 2006. "Impact of debris flows and turbidity currents on seafloor structures." *Norw. J. Geol.* 86 (3): 317–337.

Das, H. S. 2012. *Mass gravity flow analyses (Gorgon expansion project).* Rep. to Fugro Corporation. Houston: Fugro Geoconsulting.

Herschel, W. H., and R. Bulkley. 1926. "Konsistenzmessungen von Gummi-Benzollösungen." *Kolloid Zeitschrift* 39 (4): 291–300. https://doi.org/10.1007/BF01432034.

Ingarfield, S., M. Sfouni-Grigoriadou, C. de Brier, and B. Spinewine. 2016. "The importance of soil characterization in modelling sediment density flows." In *Proc., Offshore Technology Conf.* Houston: Offshore Technology Conference.

Kinash, O., and M. Najafi. 2012. "Large-diameter pipe subjected to landslide loads." *J. Pipeline Syst. Eng. Pract.* 3 (1): 1–7. https://doi.org/10.1061/(ASCE)PS.1949-1204.0000091.

Kouretzis, G. P., D. K. Karamitros, and S. W. Sloan. 2015. "Analysis of buried pipelines subjected to ground surface settlement and heave." *Can. Geotech. J.* 52 (8): 1058–1071. https://doi.org/10.1139/cgj-2014-0332.

Liu, J., J. Tian, and P. Yi. 2015. "Impact forces of submarine landslides on offshore pipelines." *Ocean Eng.* 95 (Feb): 116–127. https://doi.org/10.1016/j.oceaneng.2014.12.003.

Parker, E. J., C. Traverso, R. Moore, T. Evans, and N. Usher. 2008. "Evaluation of landslide impact on deep water submarine pipelines." In *Proc., Offshore Technology Conf.* Houston: Offshore Technology Conference.

Pazwash, H., and J. M. Robertson. 1975. "Forces on bodies in Bingham fluids." *J. Hydraul. Res.* 13 (1): 35–55. https://doi.org/10.1080/00221687509499719.

Pirmez, C., J. Marr, C. Shipp, and F. Kopp. 2004. "Observations and numerical modeling of debris flows in the Na Kika Basin, Gulf of Mexico." In *Proc., Offshore Technology Conf.* Houston: Offshore Technology Conference.

Qian, X., and H. S. Das. 2019. "Modeling subaqueous and subaerial muddy debris flows." *J. Hydraul. Eng.* 145 (1): 04018083. https://doi.org/10.1061/(ASCE)HY.1943-7900.0001526.

Randolph, M. F., D. Seo, and D. J. White. 2010. "Parametric solutions for slide impact on pipelines." *J. Geotech. Geoenviron. Eng.* 136 (7): 940–949. https://doi.org/10.1061/(ASCE)GT.1943-5606.0000314.

Randolph, M. F., and D. J. White. 2012. "Interaction forces between pipelines and submarine slides: A geotechnical viewpoint." *Ocean Eng.* 48 (Jul): 32–37. https://doi.org/10.1016/j.oceaneng.2012.03.014.

Sahdi, F., C. Gaudin, D. J. White, N. P. Boylan, and M. F. Randolph. 2014. "Centrifuge modelling of active slide–pipeline loading in soft clay." *Geotechnique* 64 (1): 16–27. https://doi.org/10.1680/geot.12.P.191.

Shcapery, R. A., and W. A. Dunlap. 1978. "Prediction of storm-induced sea bottom movement and platform forces." In *Proc., Offshore Technology Conf.* Houston: Offshore Technology Conference.

Spinewine, B., D. Rensonnet, T. De Thier, M. Clare, G. Unterseh, and H. Capart. 2013. "Numerical modeling of runout and velocity for slide-induced submarine density flows-a building block of integrated geohazards assessment for deepwater developments." In *Proc., Offshore Technology Conf.* Houston: Offshore Technology Conference.

Towhata, I., and T. M. Al-Hussaini. 1988. "Lateral loads on offshore structures exerted by submarine mudflows." *Soils Found.* 28 (3): 26–34. https://doi.org/10.3208/sandf1972.28.3_26.

Wieghardt, K. 1975. "Experiments in granular flow." *Annu. Rev. Fluid Mech.* 7 (1): 89–114. https://doi.org/10.1146/annurev.fl.07.010175.000513.

Yuan, F., L. Li, Z. Guo, and L. Wang. 2015. "Landslide impact on submarine pipelines: Analytical and numerical analysis." *J. Eng. Mech.* 141 (2): 04014109. https://doi.org/10.1061/(ASCE)EM.1943-7889.0000826.

Yuan, F., L. Wang, Z. Guo, and R. Shi. 2012a. "A refined analytical model for landslide or debris flow impact on pipelines. I: Surface pipelines." *Appl. Ocean Res.* 35 (Mar): 95–104. https://doi.org/10.1016/j.apor.2011.12.001.

Yuan, F., L. Wang, Z. Guo, and Y. Xie. 2012b. "A refined analytical model for landslide or debris flow impact on pipelines. II: Embedded pipelines." *Appl. Ocean Res.* 35 (Mar): 105–114. https://doi.org/10.1016/j.apor.2011.12.002.

Zakeri, A. 2009. "Review of state-of-the-art: Drag forces on submarine pipelines and piles caused by landslide or debris flow impact." *J. Offshore Mech. Arct.* 131 (1): 014001. https://doi.org/10.1115/1.2957922.

Zakeri, A., B. Hawlader, and K. Chi. 2012. "Drag forces caused by submarine glide block or out-runner block impact on suspended (free-span) pipelines." *Ocean Eng.* 47 (Jun): 50–57. https://doi.org/10.1016/j.oceaneng.2012.03.016.

Zakeri, A., K. Høeg, and F. Nadim. 2008. "Submarine debris flow impact on pipelines. I: Experimental investigation." *Coastal Eng.* 55 (12): 1209–1218. https://doi.org/10.1016/j.coastaleng.2008.06.003.

Zakeri, A., K. Høeg, and F. Nadim. 2009. "Submarine debris flow impact on pipelines. II: Numerical analysis." *Coastal Eng.* 56 (1): 1–10. https://doi.org/10.1016/j.coastaleng.2008.06.005.